

PRELIMINARY TESTS ON NON-METRIC CAMERA SELF-CALIBRATION BY USING WAVELET ADDITIONAL PARAMETERS

Jun-Fu Ye (1), Jaan-Rong Tsay (2)

¹ Dept. of Geomatics, National Cheng Kung University, Taiwan, Email: junfu.ye@gmail.com

² Dept. of Geomatics, National Cheng Kung University, Taiwan, Email: tsayjr@mail.ncku.edu.tw

KEY WORDS: bundle adjustment, function approximation, image distortion, photogrammetry

ABSTRACT: Camera self-calibration is the most famous and flexible technique in the field of photogrammetry to estimate the lens distortion of cameras. Over the past decades, many algebraic polynomial additional parameter models have been proposed to calibrate analogue cameras. These traditional additional parameter models are also used to calibrate diverse modern new types of digital cameras although they might not be adequate to express their lens distortion accurately. Moreover, many traditional additional parameters might be highly correlated with interior orientation parameters or other correction parameters. In our previous preliminary studies, a new camera self-calibration technique has been designed based on wavelet additional parameters (WAPs), and this model is helpful to express and correct the systematic distortion errors of images taken by metric digital cameras. Also, some preliminary tests for non-metric cameras are shown and discussed in this paper.

1. INTRODUCTION

Camera calibration is a major issue in photogrammetry, and it is used to estimate the interior orientation parameters of cameras. Nowadays, self-calibration is the most famous and flexible technique for automatically selecting additional parameters through statistical tests to estimate the systematic error components of image distortion. These additional parameters proposed in many early studies are based on mathematics or physical phenomena to establish the image distortion models. The most classic physical self-calibration model was originally proposed by Brown (1971) to calibrate close-range cameras, and Brown (1976) expanded this model to calibrate the single-head analogue aerial cameras. Some conventional mathematical self-calibration models, such as those by Ebner (1976), El-Hakim & Faig (1977), and Grün (1978), were built by using second order algebraic polynomials, spherical harmonics, and fourth order algebraic polynomials, respectively. These traditional self-calibration models help to improve the external accuracy of photo triangulation, but they also have problems of high correlations and over-parameterization (Kilpelä, 1981; Clarke and Fryer, 1998). In the digital era, these traditional self-calibration models are also in general adopted to calibrate diverse modern new types of digital cameras although they might not be suitable for accurately calibrating all kinds of cameras (Fritsch, 2015).

A family of Legendre self-calibration additional parameters was proposed by Tang et al. (2012a) to calibrate the digital frame-format airborne cameras, and they are effective and flexible in calibrating image distortion. In addition, the correlation between Legendre additional parameters is lower than the physical additional parameters. However, all unknown parameters are still not fully independent. Tang (2012b) proposed a series of self-calibration additional parameters based on Fourier series. This Fourier self-calibration model, which has the advantages of orthogonal, mathematically rigorous, flexible, generic and efficient calibration of the image distortion of all digital frame-format airborne cameras, overcomes the shortcomings of those traditional algebraic polynomials models. Unfortunately, the lens distortion signals in diverse modern new types of digital cameras might be stationary and/or non-stationary. In our previous studies, we have designed and developed a new camera self-calibration technique by using WAPs. This wavelet self-calibration model has been further improved for good stability, and some tests for a metric digital aerial camera are given in this paper. In addition, this paper also shows some preliminary tests for a non-metric digital camera.

2. METHODOLOGY

In the Cartesian coordinate system of Euclidean space, the mathematical relationship between the image space coordinates and the object space coordinates can be represented by the photogrammetric collinearity condition equations (1), where x and y are the photo coordinates; X , Y , and Z are the object coordinates; X_0 , Y_0 , and Z_0 are the

object coordinates of exposure station; f is the focal length (or principal distance) of the camera; x_0 and y_0 are the photo coordinates of the principal point; r 's are the rotation matrix terms; Δx and Δy are the systematic error components in the photo coordinates x and y ; ε_x and ε_y are the random error components in the photo coordinate observations x and y (Wolf and Dewitt, 2000).

$$\begin{aligned} x &= x_0 - f \frac{r_{11}(X - X_0) + r_{12}(Y - Y_0) + r_{13}(Z - Z_0)}{r_{31}(X - X_0) + r_{32}(Y - Y_0) + r_{33}(Z - Z_0)} + \Delta x + \varepsilon_x \\ y &= y_0 - f \frac{r_{21}(X - X_0) + r_{22}(Y - Y_0) + r_{23}(Z - Z_0)}{r_{31}(X - X_0) + r_{32}(Y - Y_0) + r_{33}(Z - Z_0)} + \Delta y + \varepsilon_y \end{aligned} \quad (1)$$

In this paper, the third-order asymmetric Daubechies wavelets are chosen as the kernel functions of the self-calibration model to approximate the systematic error components of the image distortion signals. Therefore, Δx and Δy in (1) can be expressed as (2), where x and y are the photo coordinates; W and H are the width and height of the image; s_x and s_y are the scale factors of the kernel functions in the x and y direction, respectively; ϕ_N is the father wavelet function of N th order asymmetric Daubechies wavelets; a_{ij} and b_{ij} are wavelet self-calibration additional parameters in Δx and Δy ; i and j are the translation parameters of the wavelet functions in the x and y direction, respectively. The total number of wavelet self-calibration additional parameters depends on the definition of the aforementioned parameters. The father wavelet function of asymmetric Daubechies wavelets used in this study can be given in (3), where h_n , $\forall n$, are the low-pass filtering coefficients (Daubechies, 1992).

$$\begin{aligned} \Delta x &= \Delta x(x, W, H, s_x, N, \phi_N, a_{ij}) \\ \Delta y &= \Delta y(y, W, H, s_y, N, \phi_N, b_{ij}) \end{aligned} \quad (2)$$

$$\phi(x) = \sqrt{2} \sum_{n=0}^{2N-1} h_n \phi(2x - n) \quad (3)$$

The wavelet self-calibration additional parameters used to describe the image distortion field are selected fully automatically by statistical tests, including correlation test, significance test and total correlation test (Kruck, 2016).

3. TEST DATA AND RESULTS

The two sets of test images used in this study are taken with a metric digital aerial camera and a non-metric digital camera, respectively, over the same test area shown in Figure 1. This area is an aerial camera calibration field located in Nangang, Nantou County, Taiwan.



Figure 1. Location of the test area in Taiwan and its image coverage

3.1 Metric digital aerial camera

The first camera is the UltraCam XP-Wide-Angle camera, which is a high-resolution metric digital aerial camera. The parameters of test images taken with UltraCam-XP are shown in Table 1. A total of 30 aerial images used in

this section were provided by GeoForce Technologies Co., Ltd. There are three test cases in this section: the first uses 6 images arranged in the north-south flight strips with 60% endlap and 25% sidelap; the second uses 6 images arranged in the east-west flight strips with 60% endlap and 25% sidelap; the third uses 30 images arranged in the cross strips with 80% endlap and 60% sidelap. All tie points used in three cases are overlaid in the image frame and shown in Figure 2. Each test case calculates the bundle block adjustment, including without additional parameters (Case 1-1, 2-1, and 3-1) and by using wavelet self-calibration additional parameters (Case 1-2, 2-2, and 3-2). Table 2 shows the computation parameters and test results in all cases. In all three cases, the posterior standard deviation of unit weight is significantly improved after using the wavelet additional parameters. Figure 3 illustrates the accuracy estimations of ground point coordinates, including full ground control points, full check points, and pass points (new ground control points determined by AT). The vectors of horizontal coordinate differences and elevation differences on all check points are shown in Figure 4 and Figure 5, respectively. The results indicate that Case 3 is much better than Case 1 and Case 2 although it still has some local systematic errors in the elevation differences. Figure 6 demonstrates the average residual vector of photo coordinates in each local area of 9×13 grids for each case after using WAPs.

Table 1. The parameters of test images taken with metric digital aerial camera

Acquisition Date	2012/09/21
Camera	UltraCam Xp-Wide-Angle
Focal Length	70.500 ± 0.002 mm
Pixel Size	6.0 μ m
Image Size	11310 pixels \times 17310 pixels
End lap	$\approx 80\%$
Side lap	$\approx 60\%$
Height (AGL)	≈ 545 m
Groundel Size	≈ 4.60 cm
Image Scale	$\approx 1:7700$
Calibration Field Size	750 m \times 600 m
Ground Coverage	≈ 1433 m \times 1433 m

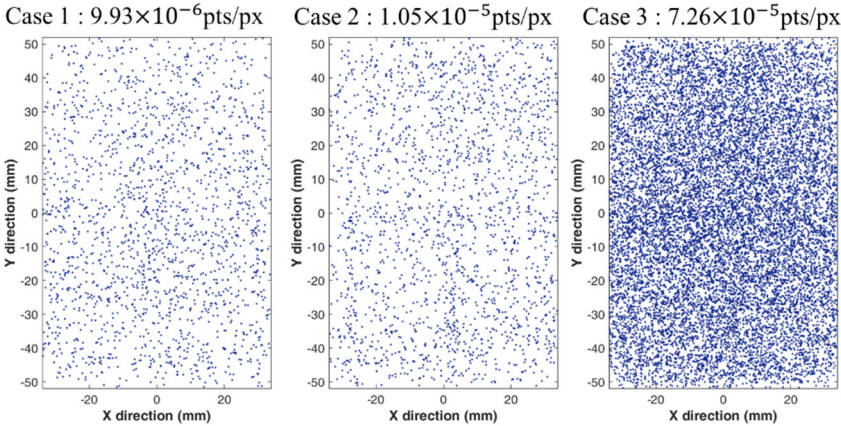
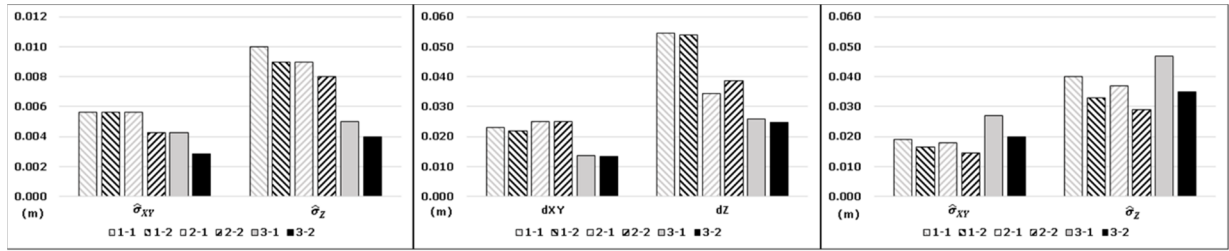


Figure 2. Overlaying all image points in the image frame

Table 2. The computation parameters and test results in all cases of metric digital camera

Case	Scale Factor (sx/sy)	Number of additional parameters	Number of iterations	$\hat{\sigma}_0$ (μm)	Degree of freedom	Average redundancy	Calculation time
1-1	-	-	3	1.98	1401	0.36	< 1 s
1-2	0.65/0.63	49/234	3+7	1.64	1325	0.34	3 s
2-1	-	-	3	1.67	1368	0.33	< 1 s
2-2	0.65/0.63	48/234	3+8	1.34	1286	0.32	4 s
3-1	-	-	4	2.24	22644	0.80	15 s
3-2	0.65/0.63	108/234	4+8	1.64	21914	0.79	93 s



(a) The RMS of $\hat{\sigma}_{XY}, \hat{\sigma}_Z$ on all full GCPs

(b) The RMS of ground coordinate differences of all full CHKs

(c) The RMS of $\hat{\sigma}_{XY}, \hat{\sigma}_Z$ of all ground points

Figure 3. The accuracy estimations of ground point coordinates

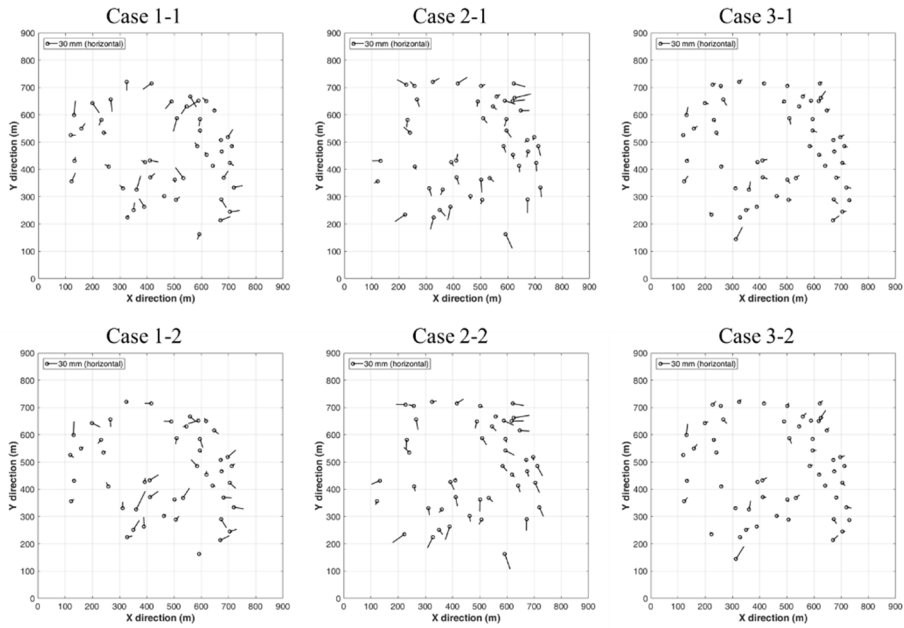


Figure 4. Vectors of horizontal coordinate differences on all check points

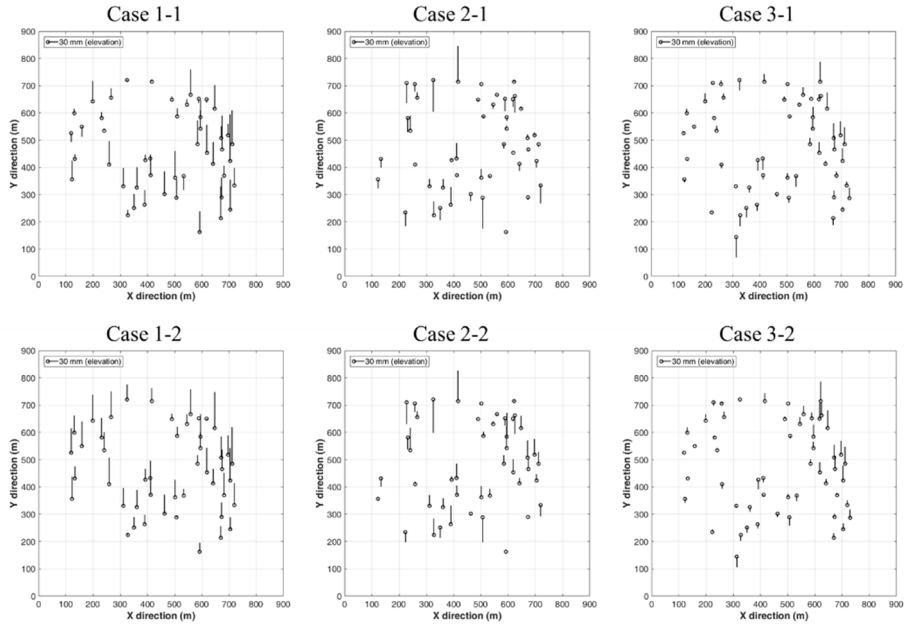


Figure 5. Vectors of elevation differences on all check points

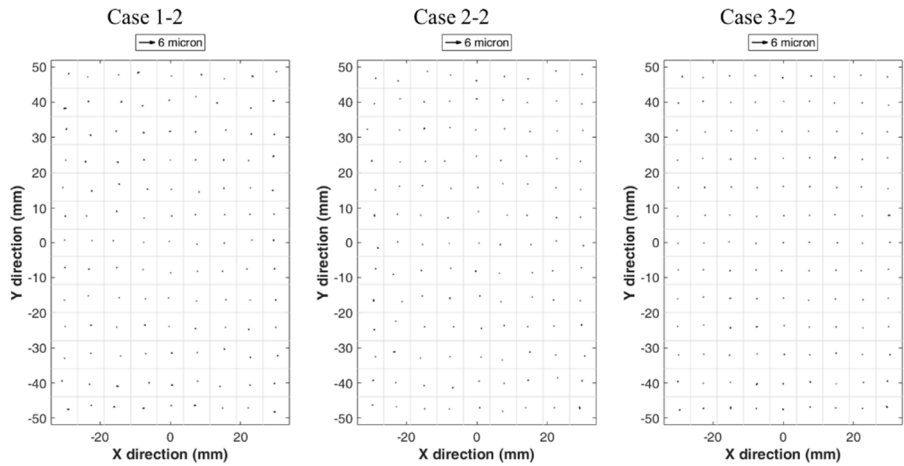


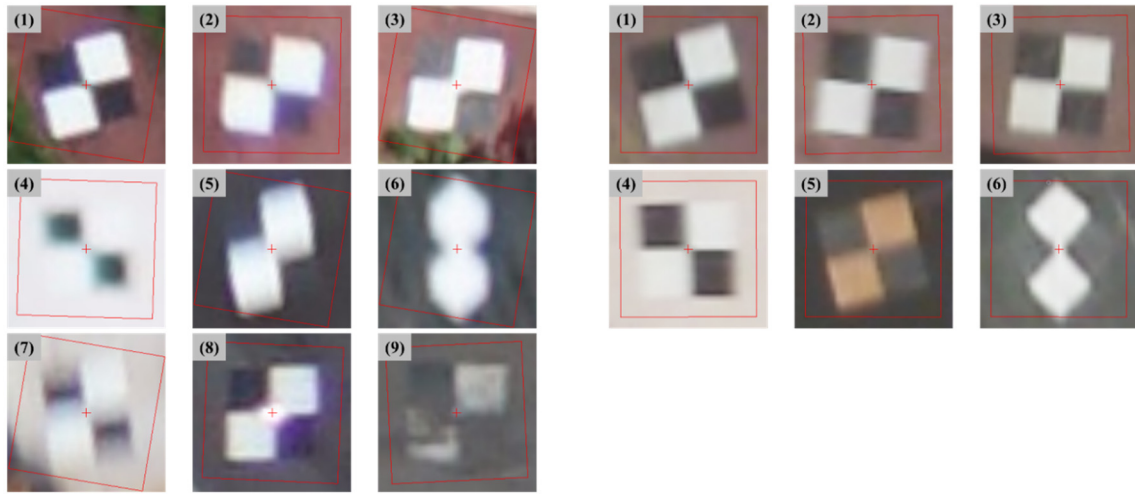
Figure 6. Average residual vectors of photo coordinate observations

3.2 Non-metric digital camera

Another set of tests is also done by using images taken with the non-metric digital camera Sony A7RII. The parameters of test images taken with Sony A7RII are shown in Table 3. Considering the efficiency of unmanned aircraft systems with this small-format camera, a total of 210 aerial images provided by Strong Engineering Consulting Co., Ltd. were stored in JPEG format. Therefore, there are some challenges in measuring the image coordinates of known points. Some sample images of ground targets from metric and non-metric digital cameras, respectively, are shown in Figure 7. The same number on the picture indicates the same ground target image taken on the closest exposure station. Some sample images were selected to calculate their blur parameter values and modulation transfer function (MTF) values, and the results are shown in Table 4. The results of the bundle block adjustment without additional parameters (Case 4-1) and by using wavelet self-calibration additional parameters (Case 4-2) are shown in Table 5. The posterior standard deviation of unit weight is significantly improved after using the wavelet additional parameters. However, the vectors of horizontal coordinate differences and elevation differences on all check points shown in Figure 8 indicate that there are still some blunders in the adjustment results. Furthermore, it also denotes the requirement on image quality for the self-calibrated bundle block adjustment.

Table 3. The parameters of test images taken with non-metric digital camera

Acquisition Date	2018/08/14
Camera	Sony A7RII
Focal Length	35 mm
Pixel Size	4.51 μm
Image Size	7952 pixels \times 5304 pixels
End lap	$\approx 80\%$
Side lap	$\approx 60\%$
Height (AGL)	≈ 400 m
Groundel Size	≈ 5.2 cm
Image Scale	$\approx 1:11400$
Calibration Field Size	750 m \times 600 m
Ground Coverage	≈ 1000 m \times 1000 m



(a) non-metric digital camera

(b) metric digital aerial camera

Figure 7. The sample images of ground targets taken with metric and non-metric digital cameras

Table 4. Image quality test (metric and non-metric digital cameras)

Sample images of ground targets from non-metric digital camera	(1)	(5)	(6)
	Blur parameter	0.959037	0.392497
MTF	0.165953	0.405493	0.194256
Sample images of ground targets from metric digital camera	(1)	(5)	(6)
	Blur parameter	0.403311	0.314598
MTF	0.394621	0.505900	0.417027

Table 5. The computation parameters and test results in all cases of non-metric digital camera

Case	Scale Factor (sx/sy)	Number of additional parameters	Number of iterations	$\hat{\sigma}_0$ (μm)	Degree of freedom	Average redundancy	Calculation time
4-1	-	-	5	6.86	52856	0.73	45 min.
4-2	0.56/0.56	153/286	5+14	4.56	50027	0.73	193 min.

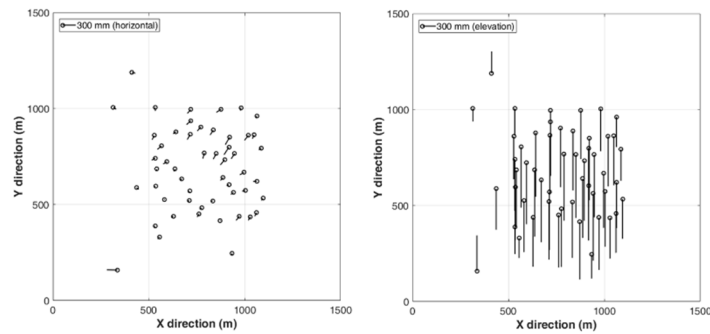


Figure 8. The difference vectors of horizontal coordinates (left) and elevations (right) on all check points (Case 4-2)

4. CONCLUSIONS

The wavelet self-calibration model proposed in our previous research works has been further improved for good stability and a better computation efficiency, and some tests on a metric digital aerial camera illustrate that the model is helpful to correct the systematic errors of image distortion. In the preliminary studies for calibrating non-metric digital cameras, the results indicate that the image quality plays an important role in the self-calibration bundle adjustment. In the future work, we will try to select and adopt only the known target points with better image quality, or give a lower weight to those target points with bad image quality.

REFERENCES

- Brown, D., 1971. Close-range camera calibration. *Photogrammetric Engineering*, 37(8), pp.855-866.
- Brown, D., 1976. The bundle method – progress and prospects. *International Archives of Photogrammetry* 21 (Part 3), pp.1-33.
- Clarke, T. and J. Fryer, 1998. The development of camera calibration methods and models. *Photogrammetric Record*, 16(91), pp.51-66.
- Daubechies, I., 1992. *Ten Lectures on Wavelets*. Society for Industrial and Applied Mathematics Philadelphia, PA, USA.
- Ebner, H., 1976. Self-calibrating block adjustment. *Bildmessung und Luftbildwesen*, 44(4), pp.128-139.
- El-Hakim, S. and W. Faig, 1977. Compensation of systematic image errors using spherical harmonics. *Proceedings of the American Society of Photogrammetry*, Fall technical meeting, Little Rock, Arkansas, pp.492-499.
- Fritsch, D., 2015. Some Stuttgart Highlights of Photogrammetry and Remote Sensing. *Photogrammetric Week 2015*, pp.3-20.
- Grün, A., 1978. Progress in photogrammetric point determination by compensation of systematic errors and detection of gross errors. *International Archives of Photogrammetry* 22 (Part 3), pp.113-140.
- Kilpelä, E., 1981. Compensation of systematic errors of image and model coordinates. *Photogrammetria* 37 (1), pp. 15-44.
- Kruck, Erwin J., 2016. *BINGO 6.8 User's manual*.
- Tang, R., D. Fritsch and M. Cramer, 2012a. New Mathematical Self-Calibration Models in Aerial Photogrammetry. 32. *Wissenschaftlich-Technische Jahrestagung der DGPF*, pp. 457-469.
- Tang, R., 2012b. A Rigorous and Flexible Calibration Method for Digital Airborne Camera Systems. *The International Archives of the Photogrammetry, Remote Sensing and Spatial Information Sciences*, XXXIX-B1, pp. 153-158.
- Wolf, P.R. and B.A. Dewitt, 2000. *Elements of Photogrammetry with Applications in GIS*. McGraw-Hill Higher Education, pp.234-235.